FLOW AROUND SINGLE AND MULTIPLE CYLINDERS

Synopsis

Submitted in Partial Fulfilment of the Requirements

For the Degree of

Doctor of Philosophy in Mechanical Engineering

By

Mr. Dhaval T Solanki
FOTE/988

Under Supervision of
Prof. Dharmendra S Sharma

Department of Mechanical Engineering,

Faculty of Technology and Engineering,

The Maharaja Sayajirao University of Baroda, Vadodara, 390 001

Gujarat, India.

February-2024

Abstract

The investigations on two-dimensional steady potential flow over single and multiple cylinders is carried out to evaluate flow parameters and hydrodynamic interaction effects. Using complex variable approach, the generalized solutions to study the effect of shapes, size, corner radius and orientation angle, and to study hydrodynamic interaction between two circular cylinders, between circular and polygonal cylinder, and between two polygonal shaped cylinders is presented. The polygonal shaped geometries with finite corner radii are obtained using hypotrochoidal mapping function. The complex potential functions are derived using Milne-Thompson circle theorem along with hypotrochoidal mapping. The uniform and non-uniform flow conditions are arrived at, by taking infinite and finite distance of vortex (or doublet) from the cylinder, respectively.

To investigate the hydrodynamic interaction between two circular cylinders, the annular area between two concentric circles is mapped conformally using bilinear transformation. The complex potential function in terms of Laurent series is used for the doublet trapped in an annulus in ζ-plane and mapped to the ξ-plane around two circles. For the study of hydrodynamic interaction between polygonal and circular cylinder, and between two polygonal cylinders the composite conformal map is developed by unique combination of bilinear and hypotrochoidal transformation. The mathematical formulas to get velocity and pressure fields around the cylinders are obtained by taking differentiation of complex potential function and mapping function. The equations for hydrodynamic forces between the cylinders are developed using Blasius theorem. The numerical results are obtained and presented to show the effects of shape, corner radii, orientation angle, flow angle, and center-to-center distance on the flow around single polygonal cylinder and the hydrodynamic interaction between polygonal cylinders. The comparison of some of the results obtained using present method is done with the results obtained from commercial CFD software package and results from the available literature.

1. Introduction

Flow around cylindrical bodies has been observed, studied, and documented by the humans since ancient time. Ancient Greeks used to play “Harp” (A triangular framed musical instrument supporting series of parallel strings) and knew that strings in the path of wind flow elicit a tone. King David hung a harp over his bed to allow it to sound by arrival of midnight breeze [1]. In 15^{th} century famous Italian artist Leonardo-da-Vinci sketched the row of vortices separating from the cylinder in the path of flow. Over the years, the field of fluid flow around cylinders has evolved from early observations and empirical insights to sophisticated theoretical models and advanced computational simulations. The complex interaction between the fluid flow and cylindrical bodies, and the intricate hydrodynamic interaction between bodies in fluid have fascinated researchers and engineers for new innovative solutions and mathematical models.

Fluid flow around single and multiple cylinders is a multifaceted and ubiquitous phenomenon with relevance in numerous fields of engineering and science. Flow around cylinders of different cross-sectional shapes (polygonal shaped cylinders) has profound implications on many applications ranging from the hydrodynamics of submerged cables, pipelines and aerodynamics of flying objects to the design of heat exchangers, suspension bridges, piers of bridges, floating platforms and the behaviour of offshore structures. In these applications, cylinders of different shapes behave as a discontinuity in fluid domain and obstruct the flow leading to change in flow parameters like velocity and pressures. Because of changes in flow parameters, the cylinders experience the hydrodynamic loads. The magnitude and nature of these hydrodynamic loads would primarily depend on the flow parameters and geometry of cylinders. In certain conditions, these hydrodynamic loads may cross the threshold limit leading to catastrophic failures of structures or mechanical members. To name some of them, the Tacoma Narrows suspension bridge in Washington collapsed in 1940 due to vibration induced by flow of air, Monju fast breeder reactor in 1995 experienced a Sodium leakage caused by the failure of a thermocouple well that was inserted into the pipe. Therefore, the exhaustive study of hydrodynamic parameters of flow over cylinders or structural/mechanical members of different cross-sections is essential. The velocity and pressure distribution, hydrodynamic forces and moments, and hydrodynamic masses are some of the very important hydrodynamic parameters to be investigated for different geometrical and flow conditions. It is important to study the effect of various geometrical parameters of cylinders (e.g. shapes, size, orientation angle, corner radii, centre distance between the cylinders, etc.) on the hydrodynamic parameters. Also, the understanding the flow patterns around the members (cylinders) and their impact on the mechanical behaviour of cylinders is crucial.

1.1 Motivation

The technical insights gained from studying hydrodynamic parameters for fluid flow around polygonal cylinders can contribute to the optimization of shapes, size, orientation and geometry of structural/mechanical members. This optimization process aims to enhance efficiency, reduce energy consumption, and improve overall performance of systems, where fluid flows across the cylinders.

In practice, the structural/mechanical members are placed close to each other in fluid flow to attain certain operational requirements. In order to meet these operational requirements against the hydrodynamic interaction effects, the behaviour of the fluid flow in various applications must be understood thoroughly to decide the optimization strategies. The comprehensive study of the interactions between the multiple polygonal cylinders in the fluid flow is very essential from structural design and safety point of view.

2. Literature Review

The fluid flow around the cylinders at very large Reynolds number ($Re \gg 10^7$), the inertia forces dominates over viscous forces and the flow behaviour is very close to that of potential

flow. The potential flow approach is based on strict assumptions of inviscid and irrotational behaviour of fluid flow ([2]). It does not show the formation and separation of viscous boundary layer from the cylinder surface. Although, some of the information can be inferred using potential flow approach, such as velocity and pressure distribution around the cylinders, steady hydrodynamic loads that cylinders experiences when placed close to each other at various distances and orientations for very large Reynolds number ($Re \gg 10^7$), and the added masses of cylinders (mechanical/structural members) can be evaluated using this approach. The potential flow theory for finding these hydrodynamic parameters around circular cylinders in inviscid incompressible flow is known for more than a century [2]. The inviscid compressible flow over circular cylinder has been investigated by Hafez and Wahba [3], Rodriguez [4], Botta [5], Pandolfi and Larocca [6], Salas [7], and Kumar and Salas [8]. The forces acting on the circular cylinder due to nearby oscillating disturbances (pulsating source, pulsating doublet and pulsating vortex) in unsteady potential flow is studied by Valentine and Madhi [9].

In the group of cylinders subjected to cross flow, the alteration/disturbances caused by each cylinder in fluid flow affects the flow parameters around the adjacent cylinders and leads to the hydrodynamic interactions. Such, hydrodynamic interactions between the members of polygonal cross sections are found in applications like floating polygonal platforms ([10], [11]), piers of bridges interacting in cross flow ([12], [13]), tubes in heat exchangers ([14], [15]), flow over two interacting aerofoils [16], marine pipelines near the sea bed ([17], [18]), thermo-wells located close to each other [19], cooling towers [20], transmission lines [21], turbine blades [22], etc. Many researchers have attempted analytical approach to investigate flow around two bodies using potential flow theory. Most of the earlier studies of potential flow in doubly connected domain are limited to simple geometries such as spheres and circular cylinders due to complex mathematical treatment involved. The problem of uniform potential flow over two parallel circular cylinders is addressed by Hicks [23] using definite integrals for complex velocity potential function. Similarly, Greenhill [24] and Carpenter [25] have provided the series solution for potential flow over two circular cylinders. Huang and Yong [26], Alassar and Ei-Gebeily [27], and Chen et al. [28] obtained the solution for potential flow around two circular cylinders using bipolar co-ordinates. Lagally [29] developed the complex potential function for flow past two-cylinders using Weierstrass function. Lagally's solution is further extended by Landweber and Shahshahan [30] to investigate hydrodynamic forces around coupled cylinders.

2.1 Potential flow around polygonal cylinders

The complex variable methods along with conformal mappings into potential flow theory can be used to study flow over flat plates [31], aerofoils [32] and other complex shaped geometries. Some of the earlier studies of potential flow over noncircular geometries have involved the use of Joukowsky [33] and Schwarz-Christoffel [34] transformation to map the region outside of a circle to the area around aerofoils and polygonal geometries, respectively. Tian and Wu [35] used Schwarz-Christoffel mapping for the investigation of inviscid flow and viscid flow (low

Reynolds number $Re < 200$) around a polygonal cylinder with even number of flat edges (N) and one of the vertices facing the free stream. They showed that, in inviscid flow the pressure-drop around the corners of polygonal cylinder is inversely proportional to the number of sides (N) of cylinder. Tian et al. [36] have further considered the flow around polygonal cylinder with odd number of edges and different orientations.

The Schwartz-Christoffel transformation is also used by Morishita [37] to study potential flow around regular polygonal cylinders of sharp corners and straight sides for $N = 3, 4$ and 6. In their study, the pressure co-efficient distribution on the surface of triangular, diamond and square shaped cylinder is obtained. It is found that maximum absolute values of velocity and pressure co-efficient at mid shoulder increases with increase of N and attain the values corresponding to the circular cylinder at very large value of N. Elcrat and Trefethen [38] have used modified Schwarz-Christoffel integral to compute Kirchhoff flow (ideal incompressible flow around an object and still wake bounded behind the object by free streamlines) around arbitrary polygonal obstacle. In their method, the parameters associated with Schwarz-Christoffel integral are handled using numerical method developed by Trefethen for Schwarz-Christoffel map. Kim and Kim [39] gave approximate analytical solution for potential flow around square cylinder using higher order multipoles. They obtained approximate solution by performing the discretization and the optimization using multiple linear regression.

2.2 Research Gap

From the literature, it is evident that the interaction between two circular cylinders has gained considerable attention of researchers. However, very few studies have been reported on the flow over interacting polygonal cylinders. Certain parameters in this problem are yet to be discussed and there is lots of scope in improvement of mathematical models, simulation strategies, and solution methodologies. To the best of authors' knowledge, the problem of potential flow around single and multiple polygonal cylinders with rounder corners, and hydrodynamic interaction between them in potential flow using complex variable method have yet not been investigated.

The effect of corner radius and side straightness of polygonal geometries on the flow parameters around the cylinders has yet not received significant attention. The use of Schwarz-Christoffel transformation to generate regular and irregular polygonal shaped geometries with rounded corners is time consuming. Also, the effect of finite radius at the corner of polygons on the flow parameters cannot be easily obtained through Schwarz-Christoffel mapping. There is a need to develop generalize solution to save computational efforts and time.

2.3 Objectives of Present Study

Following are the objectives of present study:

- To provide generalized analytical solution of potential flow around polygonal shaped cylinder with rounded corners and to study the effect of shapes, corner radii, number of sides, and orientation of polygonal cylinder on the hydrodynamic parameters (e.g. velocity and pressure).
- To investigate the hydrodynamic interaction between two polygonal cylinders in uniform potential flow and, study the effect of various geometrical parameters and flow parameters on the hydrodynamic interaction between two polygonal cylinders.

3. Mathematical Formulation

When a cylinder is placed in uniform fluid flow with free stream velocity U_∞ as shown in Figure 1, the viscous layer of fluid generates on the surface of cylinder from the stagnation point on the upstream side of cylinder (at $\theta = 0^0$). This viscous layer of fluid is known as boundary layer. The nature of boundary layer and over all fluid flow behaviour around the cylinder depends on the Reynolds number.

$$Re = \frac{\varrho U_\infty D}{\mu}. \tag{1}$$

where, U_∞ is free stream velocity, D is cylinder diameter, μ is viscosity and ϱ is density of fluid.

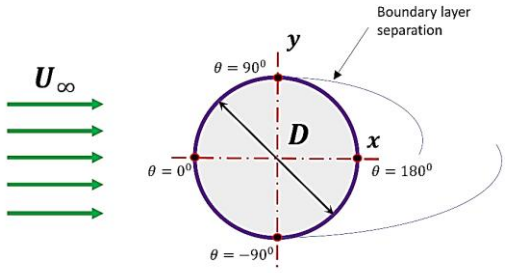

Figure 1 Uniform flow around a circular cylinder

At very large Reynold number ($Re \geq 10^7$), the inertia of fluid dominates the flow and the viscous effect can be neglected. Physically the boundary layer of fluid becomes infinitesimally thin on the surface of cylinder and the wake behind the cylinder confines to very narrowed region. These conditions resemble the solutions close to that found at zero viscosity for $Re \cong \infty$. The inviscid flow solution at zero viscosity also known as potential flow is a good approximation of flow with very large Reynolds number.

The complex variable theory is an important mathematical tool to study Potential flow. In potential flow, the flow field is described with the help of velocity potential (ϕ) and stream function (ψ). The ϕ and ψ satisfy Laplace equation ($\nabla^2\phi = 0$, $\nabla^2\psi = 0$) and in order to be holomorphic they should satisfy Cauchy- Riemann conditions,

$$\frac{\partial \phi}{\partial x} = \frac{\partial \psi}{\partial y}; \frac{\partial \phi}{\partial y} = -\frac{\partial \psi}{\partial x}. \quad (2)$$

The complex potential function for two-dimensional potential flow can be mentioned by the complex combination of velocity potential (ϕ) and stream function (ψ) as,

$$w(\zeta) = \phi(\zeta) + i\psi(\zeta). \quad (3)$$

where, $\zeta = x + iy$ is complex variable.

3.1 Potential flow around single circular cylinder

The uniform and non-uniform potential flow around a cylinder can be obtained by placing a point singularity (vortex or doublet) outside a cylinder at infinite and finite distance respectively. Such potential flow can be modelled using complex potential $g(\zeta)$ for irrotational free vortex (at $\zeta = \delta$) in unbounded fluid domain written as,

$$g(\zeta) = -\frac{i}{2\pi}\log(\zeta - \delta). \quad (4)$$

By the application of Milne-Thomson circle theorem ([40], [41]) on above function, the complex potential $w_v(\zeta, \delta)$ for the point vortex inside a unit circle can be derived,

$$w_v(\zeta, \delta) = g(\zeta) + \overline{g(\zeta)} = g(\zeta) + \overline{g(1/\bar{\zeta})}. \quad (5)$$

The function $w_v(\zeta, \delta)$ must satisfy the boundary condition such that the imaginary part of the function is constant on the boundary of cylinders,

$$Im[w_v(\zeta, \delta)] = 0, \qquad \text{on } |\zeta| = 1. \quad (6)$$

By substituting Equation (4) into Equation (5), the function $w_v(\zeta, \delta)$ is simplified as,

$$w_v(\zeta, \delta) = -\frac{i}{2\pi} log\left(\frac{\zeta - \delta}{|\delta|\left(\zeta - \frac{1}{\bar{\delta}}\right)}\right). \quad (7)$$

The above complex potential in simply connected circular domain D_ζ can be conformaly mapped to the domain D_z by using mapping $Z(\zeta) = 1/\zeta$ as shown in Figure 2.

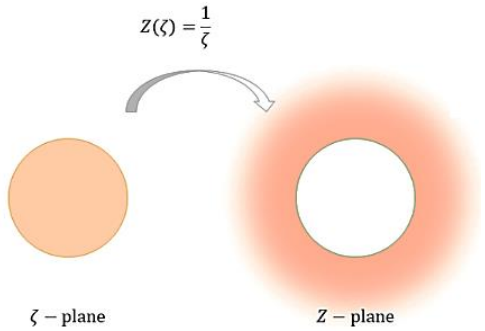

Figure 2 mapping from interior of circular cylinder to exterior of polygonal

By taking parametric derivative of complex potential function (Equation (7)) with respect to imaginary part of vortex location $\delta = \delta_R + i\delta_I$,

$$\mathcal{P}(\zeta, \delta) = U\left(\frac{1}{\zeta - \delta} + \frac{1}{2\delta} - \frac{1}{\bar{\delta}^2(\zeta - \bar{\delta}^{-1})} - \frac{1}{2\bar{\delta}}\right). \tag{8}$$

The complex potential function in Equation (8) gives uniform potential flow for a doublet at location $\delta \approx 0$ ($\delta \to 0$), and non-uniform potential flow (doublet flow) around circular cylinder for $\delta \neq 0$.

The velocity (V_c) around a cylinder can be written as,

$$V_c = u_c - iv_c = \frac{d\mathcal{P}}{d\zeta} \Big/ \frac{dZ}{d\zeta}, \tag{9}$$

where, u_c and v_c are the real and imaginary part.

By substituting complex potential function $\mathcal{P}(\zeta, \delta)$ from Equation (8) and $Z = 1/\zeta$ in above equation and differentiating with respect to ζ, complex velocity around circular cylinder is obtained as,

$$V_c = U\left(\frac{\zeta^2(2\delta\zeta + \zeta^2\bar{\delta}^2 - 2\zeta\bar{\delta} - \delta^2 - \zeta^2 + 1)}{(\zeta\bar{\delta} - 1)^2(\delta - \zeta)^2}\right). \tag{10}$$

By using Bernoulli's theorem, the pressures distribution around the circular cylinders in potential flow can be obtained in terms of non-dimensional pressure coefficient Cp as shown below,

$$Cp_c = 1 - \frac{V_c^2}{U^2} = 1 - \left(\frac{\zeta^2(2\delta\zeta + \zeta^2\bar{\delta}^2 - 2\zeta\bar{\delta} - \delta^2 - \zeta^2 + 1)}{(\zeta\bar{\delta} - 1)^2(\delta - \zeta)^2}\right)^2. \tag{11}$$

3.2 Potential flow around Polygonal cylinder

The uniform and non-uniform potential flow around polygonal shaped cylinders with rounded corners are obtained in two steps as shown in Figure 3. In first step, the interior of circle (ζ-plane) is mapped to the exterior of circle (Z-plane) using inverse map. In second step, the area around circle (Z-plane) is mapped to the area around polygon (F-plane) using hypotrochoidal map.

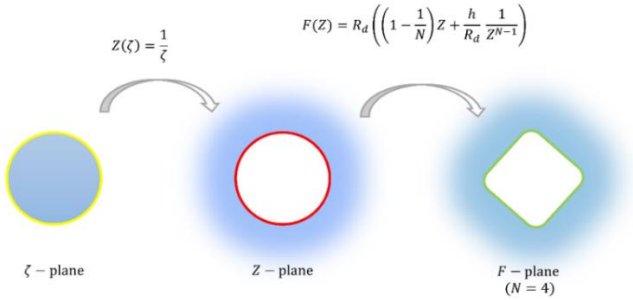

Figure 3 Composite mapping from interior of circular cylinder to exterior of polygonal shaped cylinder.

A hypotrochoid is a locus of a point on the circular lamina (generating solid circle) rolling without sliding inside another circle (directing circle). The mapping function obtained using parametric equations of hypotrochoid ([42], [43]) is given as,

$$F = f(Z) = R_d\left(\left(1-\frac{1}{N}\right)Z + \frac{h}{R_d}\ \frac{1}{Z^{N-1}}\right), \tag{12}$$

where, 'R_d' is radius of directing circle, 'R_r' is radius of rolling circle, and 'h' is distance of curve tracing point from the centre of rolling circle ($0 \leq h \leq R_r$). In order to have a closed curve, the ratio $'N'$ should be integer ($N \geq 2$).

The velocity around polygonal shaped cylinders is obtained using complex potential function $\mathcal{P}(\zeta, \delta)$ in combination with hypotrochoidal mapping (Equation (12)) as shown below,

$$V = R_d\left(1-\frac{1}{N}\right)\left(\frac{d\mathcal{P}}{d\zeta}\Big/\frac{dF}{d\zeta}\right). \tag{13}$$

By performing the differentiation and multiplying with $R_d(1-1/N)$ to avoid dependency of velocity on the size of cylinder,

$$V = \frac{-R_d\,|V_c|\,(e^{i\gamma})^N}{-R_d\,(e^{i\gamma})^N + h\,N\ \zeta^N}. \tag{14}$$

The equation of pressure co-efficient Cp around polygonal shaped cylinders can be written as follows using Bernoulli's relation (Equation (11)),

$$Cp = 1 - \left(\frac{R_d\, V_c(e^{i\gamma})^N}{U\,(-R_d\,(e^{i\gamma})^N + \,h\,N\,\,\zeta^N)}\right)^2. \tag{15}$$

3.3 Potential flow around two circular cylinders

In order to investigate the hydrodynamic interaction between two circular cylinders, the concentric annular area between two circles $q \le |\zeta| \le 1$ in ζ-plane is conformally mapped to the area outside circles $C_1'(|\xi| = 1)$ and $C_2'(|\xi - H| = R_1)$ in physical ξ-plane as shown in Figure 4 by using following bilinear conformal mapping,

$$\xi_j = \frac{\zeta_j - \lambda}{\zeta_j \lambda - 1}, \tag{16}$$

where,

$$\lambda = \frac{1}{2H}\left(H^2 + 1 - R_1^2 + \sqrt{(H^2 - (1+R_1)^2)(H^2 - (1-R_1)^2)}\right);\; q = \frac{R_1 + H - \lambda}{\lambda(R_1+H) - 1};\; (H > 1 + R_1).$$

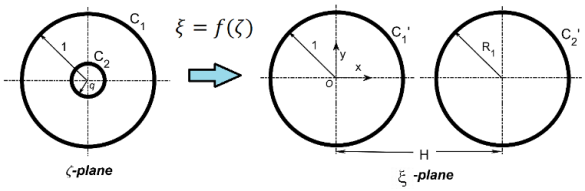

Figure 4 Annulus formed between circle of radius 1 and q in ζ-plane is mapped to two circles in ξ-plane using bilinear mapping.

The complex potential function for a singularity (vortex) trapped at $\zeta = \delta$ in an annulus domain formed between two concentric circles $\zeta_1 = e^{i\theta}$ and $\zeta_2 = qe^{i\theta}$is presented as ([41]),

$$w_v(\zeta, \delta) = \frac{1}{2\pi i} log\left(\frac{|\delta| P(\zeta\delta^{-1}, q)}{P(\zeta\bar{\delta}, q)}\right), \tag{17}$$

where, the P-function can be written in form of Laurent series expansion as shown below,

$$P(\zeta, q) = \left(\frac{\prod_{n=1}^{\infty}(1+q^{2n})^2}{\sum_{n=0}^{\infty} q^{n(n-1)}}\right) \sum_{n=-\infty}^{\infty} (-1)^n\, q^{n(n-1)}\, (\zeta)^n. \tag{18}$$

By differentiating the function $w_v(\zeta, \delta)$ (Equation (17)) with respect to δ, the complex potential function for doublet at $\zeta = \delta$ in ζ-plane corresponds to the uniform potential flow in Z-plane can be written as,

$$w_U(\zeta, \delta) = 2\pi U i a\left(e^{-i\alpha}\frac{\partial w_v(\zeta, \delta)}{\partial \delta} - e^{i\alpha}\frac{\partial w_v(\zeta, \delta)}{\partial \bar{\delta}}\right), \tag{19}$$

where, 'α' is flow angle and 'a' is a real constant associated with conformal mapping.

After substituting complex potential function w_v (Equation (17)) and constant 'a' obtained by evaluating bilinear mapping (Equation (16)) at pole $\zeta_j = 1/\lambda$,

$$w_U(\zeta_j, \delta) = \left(\frac{1}{\lambda^2} - 1\right)\frac{U}{\delta}\left[i\,sin\alpha + \left(e^{-i\alpha}\,\frac{\zeta\delta^{-1}P_\zeta(\zeta\delta^{-1}, q)}{P(\zeta\delta^{-1}, q)} - e^{i\alpha}\,\frac{\zeta\delta P_\zeta(\zeta\delta, q)}{P(\zeta\delta, q)}\right)\right], \tag{20}$$

where, $P_\zeta(\zeta\delta, q)$ and $P_\zeta(\zeta\delta^{-1}, q)$ are the differentiation of P-function with respect to the first argument of function,

$$P_\zeta(\zeta, q) = \left(\frac{\prod_{n=1}^{\infty}(1+q^{2n})^2}{\sum_{n=0}^{\infty} q^{n(n-1)}}\right)\sum_{n=-\infty}^{\infty}(-1)^n\, q^{n(n-1)}\, n(\zeta)^{n-1}, \tag{21}$$

In above formulation of complex potential function, the value of $\delta = 1/\lambda$ maps uniform potential flow around the cylinder pairs.

By performing the differentiation of complex potential $w_U(\zeta, \delta)$ (Equation (20)) and bilinear mapping (Equation (16)), the complex velocity and pressure co-efficient are written as,

$$V = -\frac{U}{\delta}\left(\frac{\left(\zeta_j\lambda - 1\right)^2}{\lambda^2}\right)\left[\left(\mathrm{e}^{-i\alpha}\{T_1(\zeta_j\delta^{-1}, q) - T_2(\zeta_j\delta^{-1}, q)\} - \mathrm{e}^{i\alpha}\{T_1(\zeta_j\delta, q) - T_2(\zeta_j\delta, q)\}\right)\right]. \tag{22}$$

$$Cp_j = 1 + \frac{1}{\delta^2}\left(\frac{\left(\zeta_j\lambda - 1\right)^4}{\lambda^4}\right)\left[\begin{pmatrix}\mathrm{e}^{-i\alpha}\{T_1(\zeta_j\delta^{-1}, q) - T_2(\zeta_j\delta^{-1}, q)\} \\ -\mathrm{e}^{i\alpha}\{T_1(\zeta_j\delta, q) - T_2(\zeta_j\delta, q)\}\end{pmatrix}\right]^2. \tag{23}$$

where,

$$T_1(\zeta\delta^{-1}, q) = \frac{\zeta_j\delta^{-2}P_{\zeta\zeta}(\zeta_j\delta^{-1}, q) + \delta^{-1}P_\zeta(\zeta_j\delta^{-1}, q)}{P(\zeta_j\delta^{-1}, q)};\; T_2(\zeta\delta^{-1}, q) = \frac{\zeta_j\delta^{-2}P_\zeta^2(\zeta_j\delta^{-1}, q)}{P^2(\zeta_j\delta^{-1}, q)};$$

$$T_1(\zeta\delta, q) = \frac{\zeta_j\delta^{2}P_{\zeta\zeta}(\zeta_j\delta, q) + \delta P_\zeta(\zeta_j\delta, q)}{P(\zeta_j\delta, q)};\; T_2(\zeta\delta, q) = \frac{\zeta_j\delta^{2}P_\zeta^2(\zeta_j\delta, q)}{P^2(\zeta_j\delta, q)}.$$

The complex hydrodynamic force $F_{x_j} - iF_{y_j}$ acting on j^{th} circular cylinder during the hydrodynamic interaction in the fluid of density ϱ is obtained by using Blasius integral theorem, as shown in below equation,

$$F_{x_j} - iF_{y_j} = \frac{i\varrho}{2}\oint\left(\frac{dw_U}{d\xi}\right)^2 d\xi, \tag{24}$$

where, F_{x_j} is the force component along flow direction (drag force) and F_{y_j} is the force component normal to the flow direction (lift force) acting on j^{th} circular cylinder.

After substituting differentiation of complex potential function (Equation (20) and mapping function (Equation (16)),

$$F_{x_j} - iF_{y_j} = \pm\frac{i\varrho}{2}\frac{U}{\delta\lambda^2}\oint(\zeta_j\lambda - 1)^2\begin{pmatrix}\mathrm{e}^{-i\alpha}\{T_1(\zeta_j\delta^{-1}, q) - T_2(\zeta_j\delta^{-1}, q)\}\\ -\mathrm{e}^{i\alpha}\{T_1(\zeta_j\delta, q) - T_2(\zeta_j\delta, q)\}\end{pmatrix}^2 d\zeta \tag{25}$$

The forces in above equation can also be represented in terms of non-dimensional force co-efficient C_{fx_j} and C_{fy_j} as shown below,

$$C_{f_{x_j}} - iC_{f_{y_j}} = \frac{F_{x_j} - iF_{y_j}}{\frac{1}{2}\varrho U^2 D_j}, \tag{26}$$

where, D_j is the diameter of j^{th} cylinder.

3.4 Flow around Polygonal-Circular Cylinder pair

The uniform potential flow around the pair of polygonal and circular cylinder is obtained using the composition of bilinear and hypotrochoidal mapping as shown below,

$$Z_j(\zeta_j) = \left(1 - \frac{1}{N}\right)\left(\frac{\zeta_j - \lambda}{\zeta_j\lambda - 1}\right) + h\left(\frac{\zeta_j - \lambda}{\zeta_j\lambda - 1}\right)^{1-N} exp(i\gamma N), \tag{27}$$

Using above composite mapping, the annular area between two circles in ζ-plane is first mapped to the area outside two unit-circles in ξ-plane, then the area outside two circles is mapped to the area outside the pair of polygonal-circular geometry in Z-plane as shown in Figure 5.

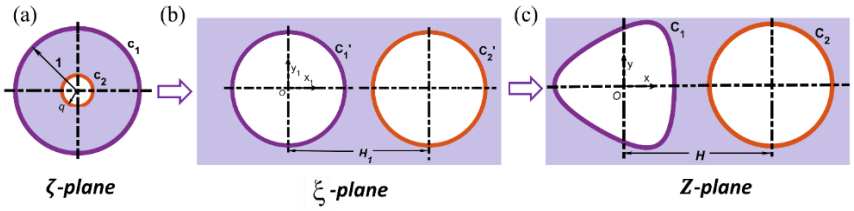

Figure 5 Annulus between the circles of unit radius and radius q in ζ-plane is mapped to the pair polygon ($N = 3$) and unit radius circle in Z-plane using composite conformal map.

By evaluating above mapping function at pole $\zeta_j = 1/\lambda$, the constant 'a' in the Equation (19) for the flow around pair of polygonal-circular cylinder can be determined as,

$$a = \left(1 - \frac{1}{N}\right)\left(\frac{1}{\lambda^2} - 1\right). \tag{28}$$

The complex potential function for doublet flow in an annulus (ζ-plane) that corresponds to the flow around polygonal-circular cylinders (Z-plane) is obtained by substituting complex potential function w_v (Equation (17)) and above constant 'a' into Equation (19) as follows,

$$w_U(\zeta,\delta)=\frac{U}{\delta}\left(1-\frac{1}{N}\right)\left(\frac{1}{\lambda^2}-1\right)\left(i\sin(\alpha)+\left(e^{-i\alpha}\,\frac{\zeta\delta^{-1}P_\zeta(\zeta\delta^{-1},q)}{P(\zeta\delta^{-1},q)}-e^{i\alpha}\,\frac{\zeta\delta P_\zeta(\zeta\delta,q)}{P(\zeta\delta,q)}\right)\right), \tag{29}$$

By taking differentiation of the above complex potential function $w_U(\zeta,\delta)$ along with composite mapping (Equation (27)), the velocity field and pressure field around the polygonal-circular cylinder pair in Z-plane can be obtained as,

$$V_j=\frac{U}{S_j\delta}\left(\mathrm{e}^{-i\alpha}\{T_1(\zeta_j\delta^{-1},q)-T_2(\zeta_j\delta^{-1},q)\}-\mathrm{e}^{i\alpha}\{T_1(\zeta_j\delta,q)-T_2(\zeta_j\delta,q)\}\right); \tag{30}$$

$$Cp_j=1-\frac{1}{S_j^2\delta^2}\left(\mathrm{e}^{-i\alpha}\{T_1(\zeta_j\delta^{-1},q)-T_2(\zeta_j\delta^{-1},q)\}-\mathrm{e}^{i\alpha}\{T_1(\zeta_j\delta,q)-T_2(\zeta_j\delta,q)\}\right)^2. \tag{31}$$

where, the terms $T_1(\zeta\delta^{-1},q), T_2(\zeta\delta^{-1},q), T_1(\zeta\delta,q)$, and $T_2(\zeta\delta,q)$ are already defined in Section 3.3 and,

$$S_j=\left(\frac{-\lambda^2(\zeta_j\lambda-1)^{N-2}}{(\zeta_j-\lambda)^N}\right)\left\{\left(\frac{\zeta_j-\lambda}{\zeta_j\lambda-1}\right)^N-hN\exp(i\gamma N)\right\}.$$

The hydrodynamic forces $F_{x_j}-iF_{y_j}$ acting on j^{th} cylinder by the fluid of density ϱ can be obtained by integrating pressure field on the cylinder boundary C_j using Blasius theorem as shown below,

$$F_{x_j}-iF_{y_j}=\mp\frac{i\varrho U^2}{2\delta^2}\left(1-\frac{1}{N}\right)\left(\frac{1}{\lambda^2}-1\right)\oint\frac{1}{S_j}\left(\begin{matrix}\mathrm{e}^{-i\alpha}\{T_1(\zeta_j\delta^{-1},q)-T_2(\zeta_j\delta^{-1},q)\}\\-\mathrm{e}^{i\alpha}\{T_1(\zeta_j\delta,q)-T_2(\zeta_j\delta,q)\}\end{matrix}\right)^2 d\zeta_j. \tag{32}$$

3.5 Flow around two polygonal cylinders

In order to investigate the hydrodynamic interaction between two polygonal cylinders, the pair of polygonal-polygonal geometry in $\boldsymbol{Z}$-plane is conformally mapped from the annulus in $\boldsymbol{\zeta}$-plane in two stages as shown in Figure 6.

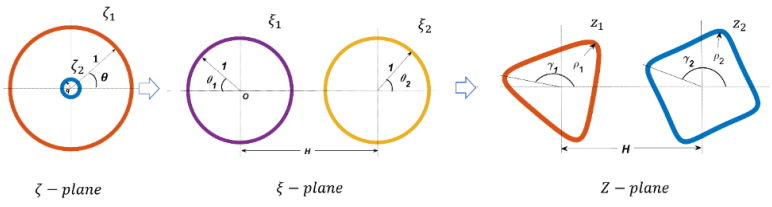

Figure 6 Mapping from annulus $q\le\zeta\le 1$ (ζ-plane) to the pair of polygonal geometries in Z-plane.

In first stage, the concentric annulus $q\le|\zeta|\le 1$ in ζ-plane is mapped onto infinite region around two non-overlapping unit-radius circles using bilinear map (Equation (16)). In second stage, two unit-circles in ξ-plane are mapped to the two-polygons in Z-plane by the application of hypotrochoidal transformation (Equation (12)).

The bilinear and hypotrochoidal mapping functions are combined to get a composite map as follows,

$$Z_j(\zeta_j) = \left[\left(1-\frac{1}{N_j}\right)\left\{\left(\frac{\zeta_j-\lambda}{\zeta_j\lambda-1}\right)-\mathcal{C}_j\right\}+h_j\left\{\left(\frac{\zeta_j-\lambda}{\zeta_j\lambda-1}\right)-\mathcal{C}_j\right\}^{1-N_j}\exp(-i\gamma_j N_j)\right]+\mathcal{C}_j, \tag{33}$$

where, $\mathcal{C}_j$ is the distance from the origin ($\mathcal{C}_1 = 0$ and $\mathcal{C}_2 = H$) of j^{th} polygonal geometry in Z-plane.

Following complex potential function is obtained for uniform potential flow around two polygonal cylinders in Z-plane by substituting $w_v(\zeta,\delta)$ from Equation (17) and constant 'a_j' (determined from mapping Equation (27)) into Equation (19),

$$w_U(\zeta\,,\delta) = \frac{U}{\delta}\left(1-\frac{1}{N_j}\right)\left(\frac{1}{\lambda^2}-1\right)\left(e^{-i\alpha}\,\frac{\zeta\,\delta^{-1}P_\zeta(\zeta\delta^{-1},q)}{P(\zeta\delta^{-1},q)}-e^{i\alpha}\,\frac{\zeta\delta P_\zeta(\zeta\delta,q)}{P(\zeta\delta,q)}\right), \tag{34}$$

By differentiating above complex potential function and composite mapping (Equation (33)), the velocity and pressure distribution on the surface of j^{th} polygonal cylinder can be written as,

$$V_j = \frac{U}{\mathcal{S}_j\delta}\begin{bmatrix}\mathrm{e}^{-i\alpha}\left(\delta^{-1}\mathcal{T}(\zeta_j\delta^{-1},q)+\frac{1}{\zeta_j}\mathcal{F}(\zeta_j\delta^{-1},q)\{1-\mathcal{F}(\zeta_j\delta^{-1},q)\}\right)\\ -\mathrm{e}^{i\alpha}\left(\delta\mathcal{T}(\zeta_j\delta,q)+\frac{1}{\zeta_j}\mathcal{F}(\zeta_j\delta,q)\{1-\mathcal{F}(\zeta_j\delta,q)\}\right)\end{bmatrix}, \tag{35}$$

and,

$$\begin{aligned}Cp_j = 1-\frac{1}{{\mathcal{S}_j}^2\delta^2}\Bigg[&\mathrm{e}^{-i\alpha}\left(\delta^{-1}\mathcal{T}(\zeta_j\delta^{-1},q)+\frac{1}{\zeta_j}\mathcal{F}(\zeta_j\delta^{-1},q)\{1-\mathcal{F}(\zeta_j\delta^{-1},q)\}\right)\\ &-\mathrm{e}^{i\alpha}\left(\delta\mathcal{T}(\zeta_j\delta,q)+\frac{1}{\zeta_j}\mathcal{F}(\zeta_j\delta,q)\{1-\mathcal{F}(\zeta_j\delta,q)\}\right)\Bigg]^2.\end{aligned} \tag{36}$$

where,

$$\mathcal{T}(\zeta_j\delta^{-1},q) = \frac{\zeta_j\delta^{-1}P_{\zeta\zeta}(\zeta_j\delta^{-1},q)}{P(\zeta_j\delta^{-1},q)};\ \mathcal{F}(\zeta_j\delta^{-1},q) = \frac{\zeta_j\delta^{-1}P_\zeta(\zeta_j\delta^{-1},q)}{P(\zeta_j\delta^{-1},q)};$$

$$\mathcal{T}(\zeta_j\delta,q) = \frac{\zeta_j\delta P_{\zeta\zeta}(\zeta_j\delta,q)}{P(\zeta_j\delta,q)};\ \mathcal{F}(\zeta_j\delta,q) = \frac{\zeta_j\delta P_\zeta(\zeta_j\delta,q)}{P(\zeta_j\delta,q)};\ \mathcal{S}_j = \frac{-\lambda^2}{(\zeta_j\lambda-1)^2}\left[1-h_j\,N_j e^{i\gamma_j N_j}\left(\frac{\zeta_j-\lambda}{\zeta_j\lambda-1}-\mathcal{C}_j\right)^{-N_j}\right].$$

Using Blasius theorem (Equation (24)), the hydrodynamic forces acting on two interacting polygonal cylinders can be determined as,

$$F_{x_j} - iF_{y_j} = \mp \frac{i\varrho U^2}{2\delta^2}\left(1 - \frac{1}{N_j}\right)\left(\frac{1}{\lambda^2} - 1\right)\oint \frac{1}{S_j}\left(\begin{matrix} \mathrm{e}^{-i\alpha}\left(\begin{matrix} \delta^{-1}\mathcal{T}\left(\zeta_j\delta^{-1}, q\right) + \\ \frac{1}{\zeta_j}\mathcal{F}\left(\zeta_j\delta^{-1}, q\right) \\ \left\{1 - \mathcal{F}\left(\zeta_j\delta^{-1}, q\right)\right\} \end{matrix}\right) \\ -\mathrm{e}^{i\alpha}\left(\begin{matrix} \delta\mathcal{T}\left(\zeta_j\delta, q\right) + \\ \frac{1}{\zeta_j}\mathcal{F}\left(\zeta_j\delta, q\right) \\ \left\{1 - \mathcal{F}\left(\zeta_j\delta, q\right)\right\} \end{matrix}\right) \end{matrix}\right)^2 d\zeta_j. \quad (37)$$

The forces F_{x_j} and F_{y_j} in above equation can be expressed in non-dimensional force coefficients $C_{f_{x_j}}$ and $C_{f_{y_j}}$ respectively.

4. Results and Discussion

The mathematical formulation for flow around single and interacting circular/polygonal cylinders are presented in previous section. This formulation is coded in MATLAB and the results are obtained to study the effects of corner radius (ρ), flow angle (α), number of sides (N), the center-to-center distance between the cylinders (H), and cylinder orientation angles (γ) on the flow parameters (e.g. velocity field, pressure profile and hydrodynamic forces) around the polygonal cylinders in uniform potential flow. Some of the results obtained using present method are compared with the results from ANSYS and from available literature for validation purpose.

4.1 Flow around Single Cylinder

The velocity and pressure distribution around circular cylinder for uniform potential flow is arrived at by using Equation (10) and (11) respectively, by taking $'\delta'$ suitably close to zero. The maximum value of velocity equal to two times the free stream velocity and the minimum value of pressure co-efficient -3 at 90° and 270^0 are obtained on the surface of cylinder in uniform potential flow. These results are in close confirmation with the maximum velocity ($V_{max}/U = 1.950$) and minimum pressure co-efficient ($Cp_{min} = -2.962$) calculated using ANSYS, and the results ($V_{max}/U = 2$ and $Cp_{min} = -3$) available from the existing literature ([2], [28], [44]).

The velocity and pressure co-efficient results are obtained for various polygonal shaped cylinders using present method and ANSYS. The comparison of one of the results is shown in Figure 7 for velocity contour around triangular cylinder ($N = 3, h = 0.1$ and $R_d = 1$). The results of present method are found in very good agreement with the results obtained from ANSYS. The maximum velocity and minimum pressure are observed at the vertex (vertices) on the line joining it (them) to the centre of polygonal cylinder, if the line is perpendicular to the flow. The fluid accelerates at this vertex (vertices) and the velocity and pressure attain their extremum values. The flow parameters around the polygonal cylinders takes the extremum values more than that around the circular cylinder.

Figure 7 Potential flow contours obtained for $N = 3, R_d = 1$, and $h = 0.1$ using (left) complex potential function along with hypotrochoidal mapping (right) inviscid flow model in ANSYS.

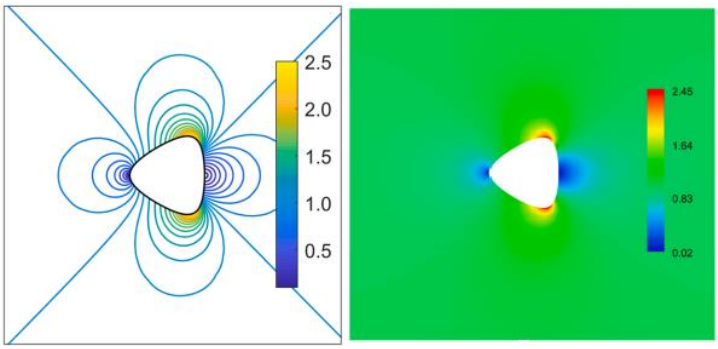

The corner radius of polygonal geometry is one of the important geometrical parameters that brings significant changes in velocity and pressure field around polygonal cylinders. The normalised corner radii ρ of polygonal cylinders can be varied from 0 to 1 and geometries ranging from hypocycloids with N cusps to circle can be obtained. For the polygons with number of sides $N \geq 3$, the effect of corner radius on maximum surface velocity and on pressure profile is shown in Figure 8. For $\rho = 0$, the absolute values of velocity and pressure co-efficient tends to infinite at cusps of hypocycloidal cylinder. The maximum surface velocity for all polygonal shaped cylinders reduces from infinity to 2.0 (two times of free stream velocity) as ρ increases from 0 to 1. The pressure co-efficient Cp for all values of $N \geq 3$ converges to -3 at $\rho = 1$ (Refer Figure 8).

Figure 8 (Left) Effect of corner radii ($0 \leq \rho \leq 1$) of polygonal cylinder on maximum velocity and (right) pressure profile on the surface of square cylinder.

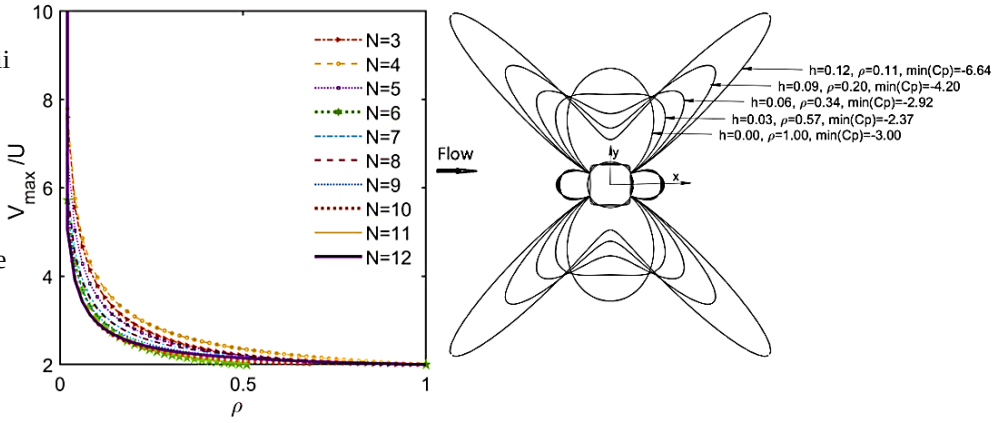

The presence of singularity such as vortex or doublet close to the cylinder (for any value of $\delta \neq 0$) gives rise to non-uniform flow around cylinder. That causes asymmetric velocity and pressure distribution on the surface of cylinders. As the value of $\delta \to 0$, the symmetrical distribution of flow parameters similar to the uniform potential flow are obtained.

4.2 Flow around Multiple cylinders

In this section the hydrodynamic interactions between two circular cylinders, between polygonal and circular cylinder, and between two polygonal cylinders are discussed. The output parameters (e.g. velocity, pressure co-efficient, and hydrodynamic forces) in these configurations are obtained by computing complex potential (Equation (17)), which is written

in terms of P-function (a form of the Laurent series). Therefore, the convergence tests of output parameters are performed to ensure the accuracy of results (Figure 9). It is observed that, the flow parameters converge after n = 4 terms. However, to ensure the accuracy of results n = 15 terms are considered in the program.

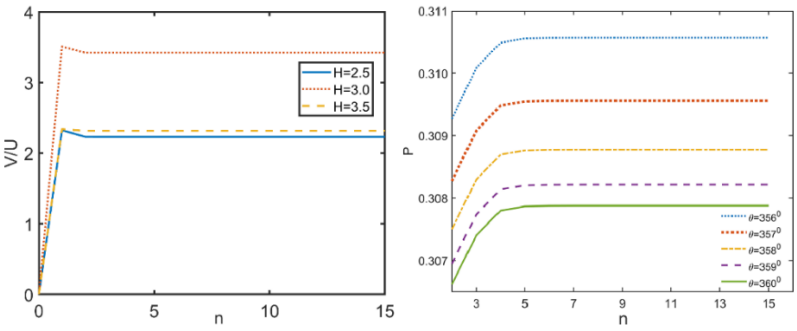

Figure 9 (Left) Convergence of velocity on the surface of triangle cylinder interacting with downstream diamond shaped cylinder, (Right) Convergence of P-function evaluated inside an annulus region.

4.2.1 Hydrodynamic interaction between two circular cylinders

The velocity and pressure field around the pair of two circular cylinders of diameter ratio D/d is investigated using mathematical formulation presented in Section 3.3. The diameter of one cylinder is kept constant ($d = 2$), while the diameter of another cylinder (D) is changed. For two identical circular cylinders ($D/d = 1$), the dimensionless pressure (P^*) is obtained as,

$$P^* = \frac{1}{2}\big(Cp(\theta) - Cp(0)\big), \tag{38}$$

where, $Cp(\theta)$ and $Cp(0)$ are pressure coefficient at angular location θ^0 and 0^0 respectively on the cylinder surface. The numerical values of normalized pressure (P^*) for the center distances $H/d = 2.5, 3, 3.5, 4, 6$ and ∞, and flow direction normal to the line connecting the centers of cylinders ($\alpha = \pi/2$) are obtained and compared with the results from ANSYS and available literature (Alassar and EI-Gabeily [27]) as shown in Figure 10. The results are found to be in close confirmation. The impact of center-to-center distances (H/d), diameter ratio (D/d) and flow angle (α) on the hydrodynamic interaction between the cylinders for various configurations are further investigated.

It is found that as center-to-center distance between the cylinders decreases, the extremum values of flow parameters (velocity and pressure) decreases in tandem configuration (flow direction along the centre line) due to the obstruction of flow between cylinders, and in side-by-side configuration (flow direction normal to the centre line) the extremum value of flow parameters increases due to Venturi effect that fluid experiences while passing between the cylinders. For large center distance ($H/d \geq 10$), the interaction effect dies out and flow parameters around the cylinders behaves similar to that around single cylinder in uniform flow.

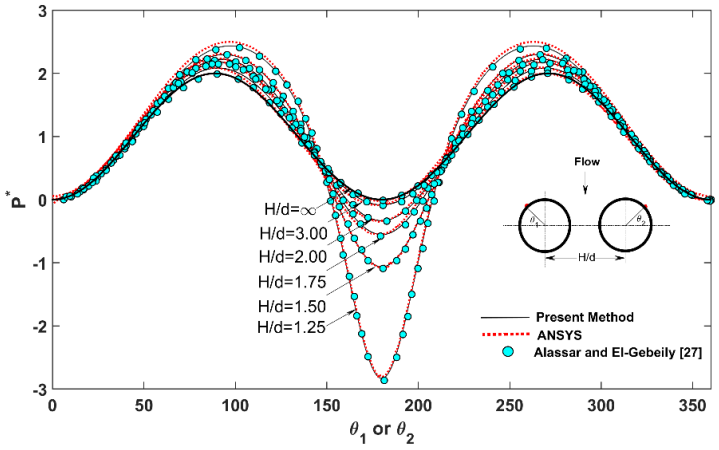

Figure 10 The dimensionless pressure P^* on the surface of two equal circular cylinders evaluated for the flow direction normal to the line connecting the centres of cylinders and for different centre distances.

The maximum velocities (V_{max}/U) and minimum pressure co-efficient (Cp_{min}) on the surface of circular cylinders in tandem configuration and in side-by-side configuration for different values of diameter ratio D/d and distance between the cylinders $H - ((D + d)/2) = 2$ are presented in presented in Table 1. With increase of diameter ratio, the magnitude of velocity and pressure co-efficient on the surface of smaller cylinder $(d = 2)$ decrease in tandem configuration and increases in side-by-side configuration. Whereas, on the surface of larger diameter cylinder the magnitude of velocity and pressure are found to increases with increase of diameter ratio for both tandem and side-by-side configurations. Also, the location (θ) of extremum values of flow parameters (velocity and pressure co-efficient) on the surface of both cylinders changes with diameter ratio.

In tandem configuration ($\alpha = 0^0$), the velocity between two interacting cylinders decreases, due to which the pressure between the cylinders increases. The increased pressure between two-cylinders results in repelling force between them along the centreline. For $\alpha = 90^0$, the velocity of flow between two interacting cylinders increases and the pressure decreases, which results in attracting forces between the cylinders along the centreline. These attractive and repelling force between the cylinders decreases with increase of center distance and vanished at center distance $H \geq 10d$ and each cylinder behaves as an individual cylinder. For $\alpha = 90^0$, the magnitudes of hydrodynamic forces are found significantly larger than $\alpha = 0^0$.

Table 1 Extremum values of flow parameters (V_{max}/U and Cp_{min}) on the surface of interacting circular cylinders in potential flow for diameter ratios $1 \leq D/d \leq 6$ and distance between cylinders $H - ((D + d)/2) = 2$.

D/d	Smaller Cylinder						Larger cylinder					
	Tandem Arrangement			Side by Side			Tandem Arrangement			Side by Side		
	V_{max}/U	Cp_{min}	θ	V_{max}/U	Cp_{min}	θ	V_{max}/U	Cp_{min}	θ	V_{max}/U	Cp_{min}	θ
1	1.8646	-2.4768	45^0	2.5939	-5.7281	180^0	1.8646	-2.4768	45^0	2.5939	-5.7281	180^0
2	1.6439	-1.7023	45^0	3.0580	-8.3517	180^0	1.9552	-2.8229	32^0	2.6902	-6.2373	180^0
3	1.4464	-1.0922	44^0	3.3459	-10.1949	180^0	1.9817	-2.9272	24^0	2.7587	-6.6105	180^0
4	1.2839	-0.6484	43^0	3.5382	-11.5187	180^0	1.9909	-2.9638	20^0	2.808	-6.885	180^0
5	1.1512	-0.3252	43^0	3.6751	-12.5066	180^0	1.9947	-2.9790	16^0	2.8448	-7.0931	180^0
6	1.0421	-0.0859	42^0	3.7775	-13.2693	180^0	1.9973	-2.9892	14^0	2.8732	-7.2554	180^0

4.2.2 Hydrodynamic interaction between polygonal and circular cylinder

The results for flow around polygonal-circular cylinder pairs are obtained for different values of center distances (H), flow angles (α), orientation angles (γ) and number of sides (N). The various pairs of polygonal-circular cylinders considered here include triangular-circular, square-circular, and diamond-circular pairs.

The minimum pressure co-efficient around various polygonal cylinders interacting with circular cylinder ($D = 2$) for the center distance $2 \leq H/D \leq 15$ and, flow angle $\alpha = 0^0$ (tandem configuration) and $\alpha = 90^0$ (side-by-side configuration) are shown in Figure 11 (b). The flow angle (α) is measured from positive real axis in counter clockwise direction (Figure 11 (a)). The magnitude of pressure co-efficient (Cp_{min}) on the interacting cylinders decreases with increase of center distance and converges towards the values correspond to the single polygonal cylinder in uniform flow. The effect of center distance ($H = 1.5D, 2.0D, 2.5D, 3.0D$ and $100D$) on velocity profile around triangular cylinder interacting with circular cylinder for $\alpha = 0^0$ is shown in Figure 11(c). The interaction effects are found significant at smaller center distances ($H/D \leq 5$). For center distance $H/D = 100$, the velocity profile is found identical to that around single triangular cylinder. The intensity of interaction also depends on the shape, size, corner radius and orientation of polygonal cylinder.

The maximum values of the velocities corresponding to different angle of attack ($0^0 \leq \alpha \leq 180^0$) and center distances ($H = 1.5D, 2.0D, 2.5D, 3.0D, 5D$ and $10D$) for some of the configurations are shown in Figure 12. These extremum values occur at some point (points) on the surface of polygonal cylinders and the locations of point (points) on the cylinders also get affected by the center distance and flow angles along with orientation of the polygonal cylinder.

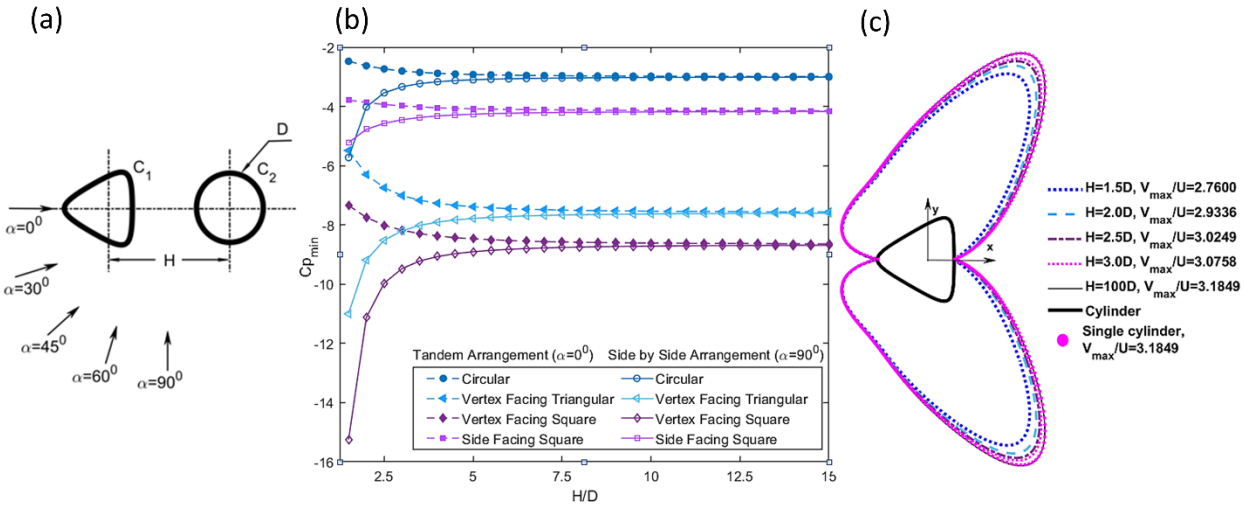

Figure 11 (a) Flow angle measurement (b) Cp_{min} around polygonal cylinder interacting with circular cylinder (c) velocity profile on triangular cylinder ($N = 3, \rho = 0.16$) interacting with circular cylinder.

It can be seen from the Figure 13 that for $H = \infty$, the flow parameters around the triangular cylinder ($N = 3, h = 0.15, \rho = 0.16$) attains the extremum value $V_{max}/U = 3.6364$ and

$Cp_{min} = -12.2231$ for flow angles $\alpha = 30^0$ and $\alpha = 90^0$ at the locations $\theta = -60^0$ and $\theta = 180^0$ respectively. The angles $\theta = -60^0$ and $\theta = 180^0$ represent orientation of the radial vector perpendicular to the flow. For the center distance $H = 1.5D$, the flow parameter attains extremum values $V_{max}/U = 3.8987$ and $Cp_{min} = -14.2003$ for $\alpha = 90^0$ at location $\theta = 180^0$, but for $\alpha = 30^0$ the values no longer remain extremum.

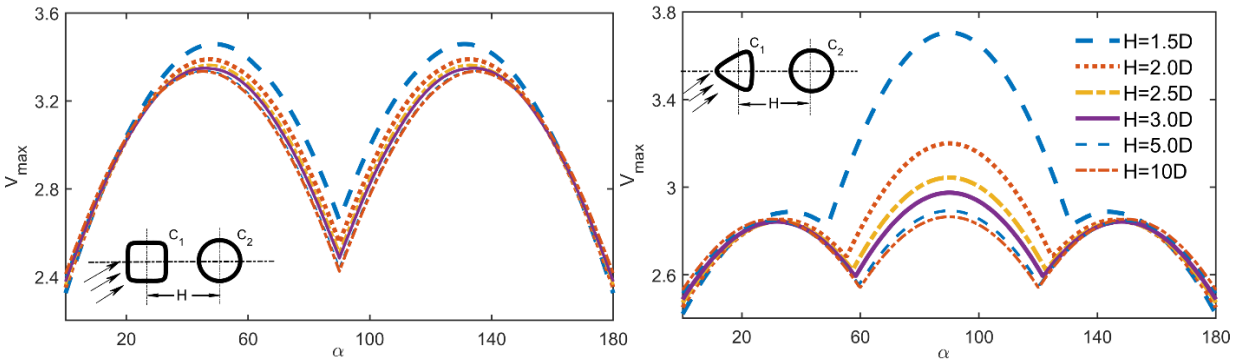

Figure 12 Maximum velocity (V_{max}/U) around polygonal cylinder interacting with circular cylinder for flow angle $0^0 \leq \alpha \leq 180^0$.

The hydrodynamic forces (C_{fx}) acting on polygonal and circular cylinder during the interaction are studied for flow angle α varying from 0^0 to 180^0. For the flow angle $\alpha = 0^0$ and $\alpha = 180^0$, the hydrodynamic forces are found to be acting in $-x$ direction on the Cylinder 1 and $+x$ direction on the Cylinder 2, i.e. forces make cylinders to repel each other. For the given finite centre distance (H/D) between the cylinders, as the flow angle increases (starting from zero), the magnitude of hydrodynamic force approaches to zero and at some threshold value of flow angle (α_1) it alters the directions and so the forces between the cylinders changes repulsive to attractive. These flow angles α_1 (change points), where sign of force co-efficients changes are shown in Table 2 for center distance $H/D = 1.5, 2.5, 5.0$ and 10, and corner radius $\rho = 0.2$. As the flow angle (α) increases beyond the change point (α_1), the magnitude of hydrodynamic forces increases and attains maximum values at $\alpha = 90^0$.

Table 2 Flow angle α_1 at which the hydrodynamic force acting on cylinders along the centerline attain zero value.

Geometry					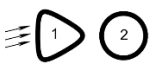								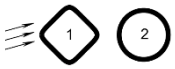							
H/D	1.5	2.5	5.0	10	1.5	2.5	5.0	10	1.5	2.5	5.0	10	1.5	2.5	5.0	10	1.5	2.5	5.0	10
α_1	36	42	44	45	31	36	43	44	42	46	46	46	34	42	44	45	38	43	45	45

4.2.3 Hydrodynamic interaction between two polygonal cylinders

The interaction behaviour between two polygonal cylinders is found similar to that discussed in previous section for pair of circular cylinders and polygonal-circular cylinder. However, the geometry affects the flow parameters significantly. The extremum values of velocity and

pressure co-efficient and their locations on two interacting polygonal cylinders are presented in Table 3 for different center distances for some of the configurations.

Table 3 Velocity and Pressure co-efficient Cp on the surface of two interacting polygonal cylinders for free stream velocity $U = 1$, corner radii $\rho_1 = \rho_2 = 0.1$.

Configuration	Center Distance (H)	Cylinder z_1			Cylinder z_2		
		V_{max}/U	Cp_{min}	θ_1	V_{max}/U	Cp_{min}	θ_2
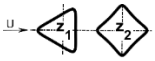	3	3.2929	-9.8437	$118.6^0, 241.4^0$	3.7162	-12.8100	$89.8^0, 270.15^0$
	5	3.6226	-12.1234	$118.5^0, 241.4^0$	3.8639	-13.9296	$89.9^0, 270^0$
	10	3.7729	-13.2349	$118.6^0, 241.4^0$	3.9616	-14.6941	$90^0, 270^0$
	3	3.7166	-12.8130	$89.8^0, 270.1^0$	2.2991	-4.2859	$132.5^0, 227.3^0$
	5	3.8639	-13.9296	$89.9^0, 270.0^0$	2.6911	-6.2421	$133.1^0, 226.8^0$
	10	3.9612	-14.6914	$89.9^0, 270.0^0$	2.8341	-7.0320	$133.2^0, 226.7^0$
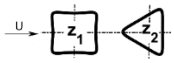	3	2.2991	-4.2859	$132.61^0, 227.3^0$	3.6535	-12.3483	$61.2^0, 298.7^0$
	5	2.6911	-6.2421	$133.1^0, 226.8^0$	3.7250	-12.8757	$61.3^0, 298.6^0$
	10	2.8341	-7.032	$133.2^0, 226.7^0$	3.7871	-13.3421	$61.3^0, 298.6^0$
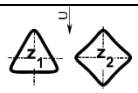	3	4.4532	-18.8361	207.7^0	5.1877	-25.9124	179.9^0
	5	4.0144	-15.1155	208.5^0	4.2616	-17.1611	179.9^0
	10	3.8610	-13.9074	208.6^0	4.0499	-15.4016	179.9^0
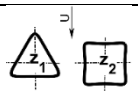	3	4.4532	-18.8362	207.7^0	3.1650	-9.0175	$43.4^0, 316.5^0$
	5	4.0144	-15.1155	208.5^0	2.9786	-7.8724	$43.3^0, 316.6^0$
	10	3.8610	-13.9074	208.6^0	2.8989	-7.4036	$43.2^0, 316.7^0$
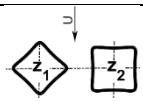	3	5.1877	-25.9124	179.9^0	3.1650	-9.0175	$43.4^0, 316.5^0$
	5	4.2557	-17.1116	179.9^0	2.9786	-7.8724	$43.3^0, 316.6^0$
	10	4.0499	-15.4016	179.9^0	2.8989	-7.4036	$43.2^0, 316.7^0$

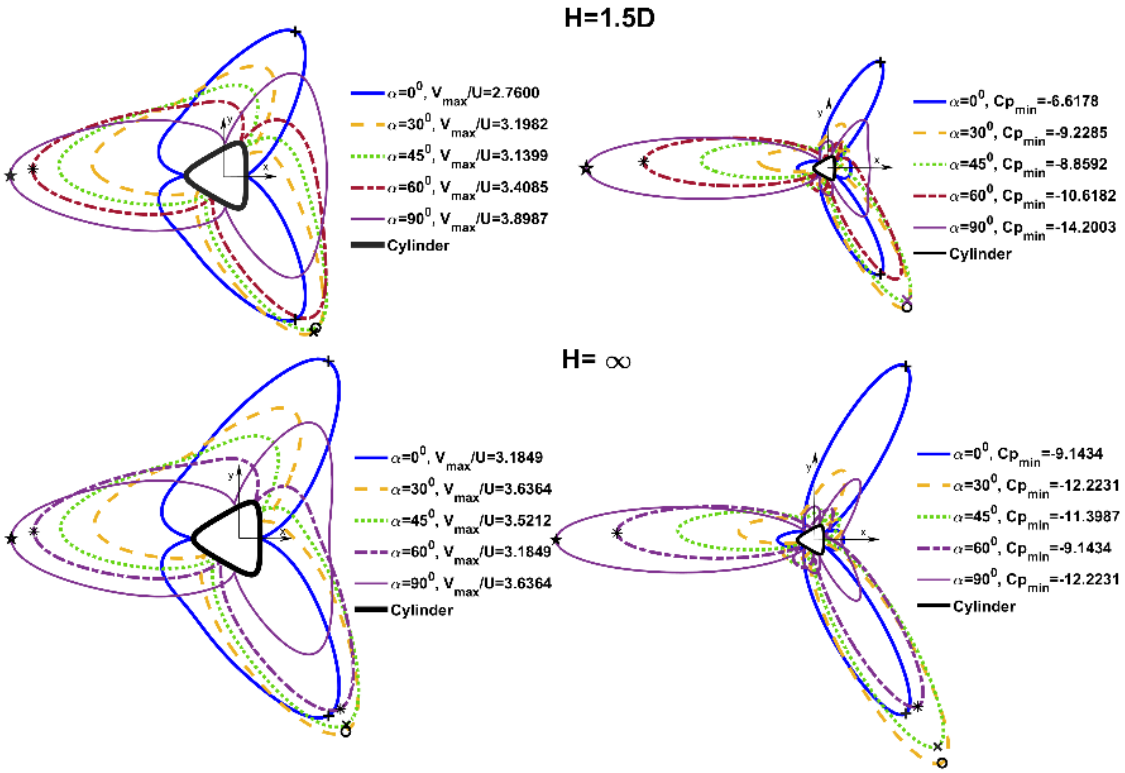

Figure 13 (left) Velocity profile and (right) Pressure profile on the surface of triangular cylinder ($N = 3, \rho = 0.16$) interacting with circular cylinder for the center distance $H = 1.5D$ and ∞ in uniform potential flow.

To study the effects of corner radii of cylinders on flow parameters, the hydrodynamic forces acting on the polygonal cylinders for centre distance $2.5 \leq H \leq 40$, corner radii $\rho_1 = \rho_2 = 0.01, 0.1$ and 1, and the flow angle $\alpha = 0^0$ are shown in Figure 14. The hydrodynamic forces

are represented in terms of non-dimensional force coefficient C_{fx} and C_{fy} for the forces acting in the x and y directions, respectively. For the given center distance and orientation, as the corner radius (ρ) decreases the hydrodynamic forces acting on polygonal cylinders increases. The hydrodynamic forces acting on cylinders increases with decrease of centre distance (H). At a large centre distance ($H \geq 10$), the forces acting on cylinders converge to zero and the interaction effect die out.

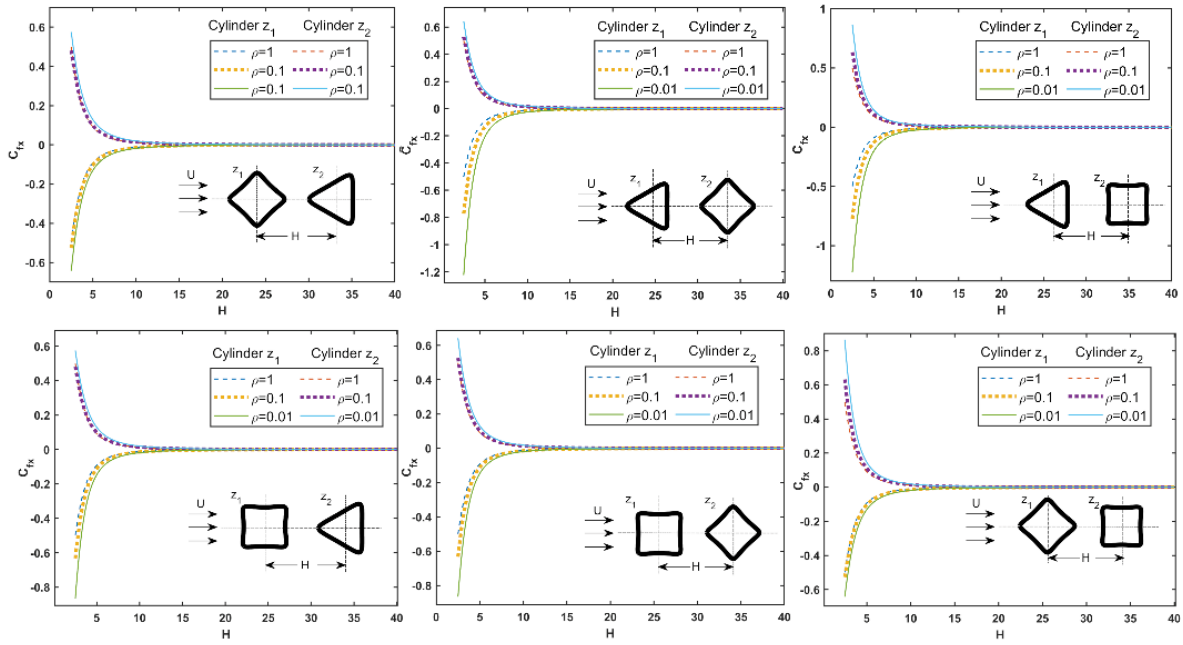

Figure 14 Hydrodynamic force (C_{fx}) acting on polygonal cylinders during interaction for centre distance $2.5 \leq H \leq 40$, flow angle $\alpha = 0^0$, corner radii $\rho_1 = \rho_2 = 0.01, 0.1$ and 1.

4.3 Summery and Conclusions

Using a complex variable approach, the potential flow around single and multiple cylinders of various polygonal shapes are investigated. The MATLAB code is prepared based on mathematical formulation and the numerical results are obtained to investigate the effects of shapes, number of sides, corner radii, orientation angle, flow angle, and center-to-center distance on the flow around single and interacting polygonal cylinders. Some of the results obtained through present method are compared with the results from existing literature and those obtained using ANSYS Fluent.

For the single cylinder problem, the area inside a circle is conformally mapped to the area outside the polygonal geometry using hypotrochoidal mapping and the numerical results are obtained. Following can be concluded.

1) The maximum velocities and minimum pressures are observed at the vertex (vertices) on the line joining it (them) to the centre of polygonal cylinder, if the line is perpendicular to the flow.

2) It is also found that as normalised corner radius ρ decreases, maximum velocity and pressure drop increases at the corners of polygonal cylinders and approaches equal to $V_{max}/U = 2,\ Cp_{min} = -3$ corresponding to a circular cylinder ($\rho = 1$).
3) At the cusp ($\rho = 0$) of hypocycloidal shaped cylinders, the maximum velocity and minimum pressure attain infinite value due to presence of singularity.
4) Number of sides (N) has significant effect on pressure co-efficient (Cp_{min}) and velocity (V_{max}/U). As $N \to \infty$, Cp_{min} and V_{max}/U approaches to -3 and 2 respectively.
5) Asymmetric velocity and pressure distribution are found around the circular and polygonal shaped cylinders for the potential flow due to the presence of doublet at finite distance from the cylinder.
6) The corner radius (ρ), orientation angle (γ), number of sides (N) and flow angle (α) are important parameters that impact on flow parameters around the cylinder.

For the hydrodynamic interaction between two cylinders, the annular area between two concentric circles ($q \leq |\zeta| \leq 1$) in ζ-plane is mapped onto infinite region around two non-overlapping polygons in Z-plane by unique combination of bilinear and hypotrochoidal transformation. The flow parameters are obtained by computing complex potential which is written in terms of Laurent series. Therefore, the convergence tests are performed and the numerical results are obtained. Following are the major conclusions for the interaction between two cylinders.

1) In uniform flow, the vicinity of one cylinder alters the flow parameters around the neighboring cylinder and the hydrodynamic interaction is observed. The maximum interaction between the cylinders are found in side-by-side configuration and the minimum interaction is observed in tandem configuration of cylinders.
2) The hydrodynamic interaction effects on the flow parameters intensifies with decrease of center to center distance between the cylinders for $H < 10$. For the center distance $H \gg 10$, no significant interaction effects are observed and the flow parameters around cylinders are found similar to the that around isolated cylinder in free stream flow.
3) Apart from the center distance, the flow angle, shape of cylinders, orientations of cylinders and the corner radii are other important parameters that affect the hydrodynamic interaction between the cylinders.
4) In tandem configuration ($\alpha = 0^0$), the hydrodynamic forces of repulsive in nature are found to be acting between the cylinders. As the flow angle increases (starting from zero), the magnitude of hydrodynamic force approaches to zero and at some threshold value of flow angle (α_1) it alters the directions and so the nature of forces between the cylinders changes from repulsive to attractive. As the flow angle (α) increases beyond α_1, the magnitude of hydrodynamic forces increases and attains maximum values at $\alpha = 90^0$.

LIST OF PUBLICATION

Journal Papers:

1) **Solanki D.T., Sharma D.S.**, "Potential flow around polygonal shaped cylinders using hypotrochoidal mapping function", International Journal of Mechanical Sciences 2022; 226: 107395. **(*Elsevier*)**
2) **Solanki D.T., Sharma D.S.**, "Hydrodynamic interaction between polygonal and circular cylinder in uniform potential flow", Journal of the Brazilian Society of Mechanical Sciences and Engineering 2023; 45: 645. doi.org/10.1007/s40430-023-04546-7. **(*Springer*)**
3) **Solanki D.T., Sharma D.S.**, "Hydrodynamic interaction between two polygonal cylinders in uniform potential flow", Ocean Engineering 2023; 286: 115674. **(*Elsevier*)**
4) **Solanki D.T., Sharma D.S.**, "Hydrodynamic interaction between to circular cylinders in uniform and non-uniform potential flow" (*To be communicated*)
5) **Solanki D.T., Sharma D.S.**, "Ground effect on the potential flow around polygonal cylinder" (*To be communicated*)

Conference Paper:

1) **Solanki, D.T., Sharma, D.S.**, "Potential Flow past Circular Cylindrical Shape Using Complex Potential Function", Proceedings of the International Conference on Contemporary Engineering and Technology, April 10-11, 2021, Chennai, India.

Book Chapter:

1) **Solanki, D.T., Sharma, D.S.**, "Potential Flow around square cylinder with rounded corners", Fluid Mechanics and Fluid Power, Volume 3. FMFP 2022. Lecture Notes in Mechanical Engineering. Springer, Singapore. **(*Springer*)**

References

[1] R. D. Blewins, *Flow-Induced Vibration*, Reprint Ed. Malabar, Florida, 2001.
[2] L. M. Milne-Thompson, *Theoretical hydrodynamics.*, 5th ed. New York: Macmillan, 1968. doi: https://doi.org/10.1007/978-1-349-00517-8.
[3] M. Hafez and E. Wahba, "Inviscid flows over a cylinder.," *Comput. Methods Appl. Mech. Eng.*, vol. 193, pp. 1981–1995, 2004, doi: https://doi.org/10.1016/j.cma.2003.12.048.
[4] O. Rodriguez, "The circular cylinder in subsonic and transonic flow," *AIAA J.*, vol. 22, pp. 1713–1718, 1984, doi: https://doi.org/10.2514/3.8842.
[5] N. Botta, "The Inviscid transonic flow about a cylinder," *J. Fluid Mech.*, vol. 301, pp. 225–250, 1995, doi: https://doi.org/10.1017/S0022112095003879.
[6] M. Pandolfi and F. Larocca, "Transonic flow about a circular cylinder," *Comput. Fluids*, vol. 17, pp. 205–220, 1989, doi: https://doi.org/10.1016/0045-7930(89)90017-0.
[7] M. D. Salas, "Recent development in transonic Euler flow over a circular cylinder," *Math. Comput. Simul.*, vol. 25, pp. 232–236, 1983, doi: https://doi.org/10.1016/0378-4754(83)

90098-8.
[8] A. Kumar and M. D. Salas, “Euler and Navier-Stokes solutions for supersonic shear flow past a circular cylinder,” *AIAA J.*, vol. 23, pp. 583–587, 1985, doi: https://doi.org/10.2514/6.1984-339.
[9] D. Valentine and F. Madhi, “Unsteady Potential Flow Theory and Numerical Analysis of Forces on Cylinders Induced by Nearby Oscillating Disturbances.,” in *Proceedings of the ASME 2009 28th International Conference on Ocean, Offshore and Arctic Engineering*, Honolulu, Hawaii, USA: Volume 6: Materials Technology; C.C. Mei Symposium on Wave Mechanics and Hydrodynamics; Offshore Measurement and Data Interpretation, 2009, pp. 631–639. doi: https://doi.org/10.1115/OMAE2009-80124.
[10] J. C. Park and C. M. Wang, “Hydrodynamic behaviour of floating polygonal platforms under wave action,” *J. Mar. Sci. Eng.*, vol. 9, no. 9, 2021, doi: 10.3390/jmse9090923.
[11] J. C. Park and C. M. Wang, “Hydrodynamic Behaviour of a Floating Polygonal Platform Centrally Placed within a Polygonal Ring Structure under Wave Action,” *J. Mar. Sci. Eng.*, vol. 10, no. 10, p. 1430, Oct. 2022, doi: 10.3390/jmse10101430.
[12] A. M. Aly and E. Dougherty, “Bridge pier geometry effects on local scour potential: A comparative study,” *Ocean Eng.*, vol. 234, Aug. 2021, doi: 10.1016/j.oceaneng.2021.109326.
[13] B. A. Vijayasree, T. I. Eldho, B. S. Mazumder, and N. Ahmad, “Influence of bridge pier shape on flow field and scour geometry,” *Int. J. River Basin Manag.*, vol. 17, no. 1, pp. 109–129, Jan. 2019, doi: 10.1080/15715124.2017.1394315.
[14] W. Tan, C. Zhao, P. Ren, Y. Wang, and G. Zhu, “Fluid elastic instability research of tube bundles by a two-way fluid-structure interaction simulation,” *Int. J. Press. Vessel. Pip.*, vol. 199, p. 104705, 2022, doi: https://doi.org/10.1016/j.ijpvp.2022.104705.
[15] N. Tran and C. C. Wang, “Effects of tube shapes on the performance of recuperative and regenerative heat exchangers,” *Energy*, vol. 169, pp. 1–17, Feb. 2019, doi: 10.1016/j.energy.2018.11.127.
[16] S. L. Lan and M. Sun, “Aerodynamic interaction of two airfoils in unsteady motion,” *Acta Mech.*, vol. 150, pp. 39–51, 2001, doi: https://doi.org/10.1007/BF01178543.
[17] K. Y. Lam, Q. X. Wang, and Z. Zong, “A nonlinear fluid-structure interaction analysis of a near-bed submarine pipeline in a current,” *J. Fluids Struct.*, vol. 16, pp. 1177–1191, 2002, doi: https://doi.org/10.1006/JFLS.2002.0463.
[18] H. R. Neto, A. Cavalini, J. M. Vedovoto, A. S. Neto, and D. A. Rade, “Influence of seabed proximity on the vibration response of a pipeline accounting for fluid-structure interaction,” *Mech. Syst. Signal Process.*, vol. 114, pp. 224–238, 2019, doi: https://doi.org/10.1016/j.ymssp.2018.05.017.
[19] Y. Zhang, L. Ding, M. Qi, and G. Bei, “Numerical Analysis of Dynamic Characteristics of Thermowell Based on Two-Way Thermo-Fluid-Solid Coupling,” *Shock Vib.*, vol. 2021, 2021, doi: 10.1155/2021/7759673.
[20] T. F. Sun and Z. F. Gu, “Interference between wind loading on a group of structures,” *J. Wind Eng. Ind. Aerodyn.*, vol. 54–55, pp. 213–225, 1995, doi: https://doi.org/10.1016/0167-6105(94)00051-E.
[21] H. Matsumiya, T. Yagi, and J. H. G. Macdonald, “Unsteady aerodynamic force modeling for 3-DoF-galloping of four-bundled conductors,” *J. Fluids Struct.*, vol. 112, p. 103581, 2022, doi: https://doi.org/10.1016/j.jfluidstructs.2022.103581.
[22] P. J. Baddoo and L. J. Ayton, “Potential flow through cascade of aerofoils: direct and inverse problems,” in *Proceedings of The Royal Society A*, 2018, p. 20180065. doi: https://doi.org/10.1098/rspa.2018.0065.
[23] W. M. Hicks, “On the motion of two-cylinders in a Fluid,” *Q. J. Pure Appl. Math.*, vol. 16, p. 113, 1879.
[24] A. G. Greenhill, “Functional Images in Cartesians,” *Q. J. Pure Appl. Math.*, vol. 18, p. 231, 1882.
[25] L. H. Carpenter, “On the motion of two-cylinders in an ideal fluid,” *J. Res. Natl. Bur. Stand. (1934).*, vol. 61, pp. 83–87, 1958.

[26] L. H. Huang and J. K. Yong, “Hybrid approach to uniform flow past two cylinders,” *J. Eng. Mech.*, vol. 121, pp. 367–378, 1995.
[27] R. S. Alassar and M. A. Ei-Gebeily, “Inviscid flow past two-cylinders,” *J. Fluids Eng. ASME*, vol. 131, p. 054501, 2009.
[28] J. T. Chen, Y. T. Chou, J. H. Kao, and J. W. Lee, “Analytical solution for potential flow across two circular cylinders using the BIE in conjunction with degenerate kernels of bipolar coordinates,” *Appl. Math. Lett.*, vol. 132, Oct. 2022, doi: 10.1016/j.aml.2022.108137.
[29] M. Lagally, “Die riebungslose Stromung im Aubengebiet zweier Kreise.,” *J. Math. Mech.*, vol. 9, pp. 299–305, 1929.
[30] L. Landweber and A. Shahshahan, “Added masses and forces on two bodies approaching central impact in an inviscid fluid,” *Res. J. Sh.*, vol. 36, pp. 99–122, 1992.
[31] C. Mahboub, N. Moummi, and A. Brima, “Potential flow over an inclined thin flat-plate,” *J. Renew. Energies*, vol. 22, pp. 251–256, 2019.
[32] M. Gaunaa, *Unsteady 2D potential-flow forces on a thin variable geometry airfoil undergoing arbitrary motion*. Denmark: Forskningscenter Risoe, 2006.
[33] H. R. Malonek and R. D. Almeida, “A note on generalized Joukowski transformation,” *Appl. Math. Lett.*, vol. 23, pp. 1174–1178, 2010, doi: https://doi.org/10.1016/j.aml.2010.05.006.
[34] T. A. Driscoll and L. N. Trefethen, *Schwarz-Christoffel mappings*. Cambridge UK: Cambridge University Press, 2002. doi: https://doi.org/10.2140/pjm.2014.270.319.
[35] Z. W. Tian and Z. N. Wu, “A study of two-dimensional flow past regular polygons via conformal mapping,” *J. Fluid Mech.*, vol. 628, pp. 121–154, 2009, doi: 10.1017/S0022112009006168.
[36] Z. W. Tian, H. Niu, and Z. Wu, “Flow past polygons with an odd number of edges,” *Sci. China Physics, Mech. Astron.*, vol. 54, no. 4, pp. 683–689, Apr. 2011, doi: 10.1007/s11433-011-4267-3.
[37] E. Morishita, “Schwartz-Christoffel Transformation applied to Polygons and Airfoils,” *Int. J. Pure Math.*, vol. 2, pp. 1–13, 2015, [Online]. Available: https://www.researchgate.net/publication/299468866
[38] R. Elcrat and N. Trefethen, “Classical free-streamline flow over polygonal obstacle,” *J. Comput. Appl. Math.*, vol. 14, pp. 251–265, 1986, doi: https://doi.org/10.1016/0377-0427(86)90142-1.
[39] E. J. Kim and I. Kim, “Approximate analytic solution of the potential flow around a rectangle,” *Am. J. Phys.*, vol. 88, pp. 25–30, Oct. 2019, doi: 10.1119/10.0000264.
[40] D. G. Crowdy, “Analytical Solution for uniform potential flow past multiple cylinders,” *Eur. J. Mech. B/Fluids*, vol. 25, pp. 459–470, 2006.
[41] D. G. Crowdy, “A new calculus for two-dimensional vortex dynamics,” in *Theoretical and Computational Fluid Dynamics*, Mar. 2010, pp. 9–24. doi: 10.1007/s00162-009-0098-5.
[42] D. S. Sharma, “Stresses around hypotrochoidal hole in infinite isotropic plate,” *Int. J. Mech. Sci.*, vol. 105, pp. 32–40, 2016, doi: https://doi.org/10.1016/j.ijmecsci.2015.10.018.
[43] N. P. Patel and D. S. Sharma, “On the stress concentration around polygonal cut-out of complex geometry in an infinite orthotropic plate,” *Compos. Struct.*, vol. 179, pp. 415–436, 2017.
[44] F. M. White, *Fluid mechanicss.*, 7th ed. New York: McGraw Hill, 2009.